

Your manuscript was typeset and received English language copy-editing.
The resulting file is available for proof-reading in the final journal style.
The present document is only to review the language changes.

The Coastal Surveillance Through Observation of Ocean Color (COAST&OOC) dataset

Philippe Massicotte¹, Marcel Babin^{4,1}, Frank Fell², Vincent Fournier-Sicre^{3,5}, and David Doxaran⁴

¹Takuvik International Research Laboratory (IRL 3376) ULaval – CNRS, Biology department,
Laval University, Quebec G1V 06A, Canada

²Informus GmbH, 13187 Berlin, Germany

³ACRI-ST, 260 Route du Pin Montard, 06904 Sophia Antipolis, France

⁴Laboratoire d’Océanographie de Villefranche, CNRS/Sorbonne Université,
06230 Villefranche-sur-Mer, France

⁵European Organisation for the Exploitation of Meteorological Satellites (EUMETSAT), EUMETSAT-Allee 1, 64295
Darmstadt, Germany

Correspondence: Marcel Babin (marcel.babin@takuvik.ulaval.ca)

Received: 8 March 2023 – Revised: 29 June 2023 – Accepted: 4 July 2023 – Published:

Abstract. **CE1 CE2 CE3** Coastal Surveillance Through Observation of Ocean Color (COAST&OOC) oceanographic expeditions were conducted in 1997 and 1998 to examine the relationship between the optical properties of seawater and related biological and chemical properties across the ~~coastal-to-open-ocean~~ coastal to open-ocean gradient in various European seas. A total of 379 stations were visited along the coasts of the Gulf of Lion in the Mediterranean Sea ($n = 61$), ~~the~~ Adriatic Sea ($n = 39$), ~~the~~ Baltic Sea ($n = 57$), ~~the~~ North Sea ($n = 99$), ~~the~~ English Channel ($n = 85$)~~and~~, ~~and the~~ Atlantic Ocean ($n = 38$). Particular emphasis was ~~dedicated to placed on~~ on the collection of a comprehensive set of apparent (AOPs) ~~and inherent~~ (IOPs) ~~optical properties and inherent optical properties~~ (AOPs and IOPs) to support the development of ocean color ~~remote-sensing~~ remote-sensing algorithms. The data were collected in situ using traditional ship-based sampling ~~, but also from a helicopter, which is a very efficient means for that type of coastal sampling. The dataset collected during~~ the COAST&OOC campaigns is unique in that it is fully consistent in terms of operators, protocols, and instrumentation. This rich and historical dataset is still today frequently requested and used by other researchers. Therefore, we present the result of an effort to compile and standardize a dataset which will facilitate its reuse in future development and evaluation of new bio-optical models adapted for ~~optically-complex~~ optically complex waters. The dataset

is available at <https://doi.org/10.17882/93570> (Massicotte et al., 2023).

1 Introduction

Since the launch of the Coastal Zone Color Scanner (CZCS) by NASA in 1978, ocean color remote sensing has been used to monitor the state of ~~, and the~~ and changes in global marine ecosystems ~~both in~~ in both time and space. In open oceans, the main component that affects the variations in the inherent (IOPs) ~~and apparent (AOPs)~~ optical properties and apparent optical properties (IOPs and AOPs) of seawater is phytoplankton, which is usually represented by the concentration of chlorophyll *a* (Morel and Prieur, 1977). Such ~~open ocean~~ open-ocean waters are traditionally termed ~~Case-1~~ Case-1 waters. Many simple spectral ~~band ratio~~ band-ratio algorithms have been developed to link changes in ~~remotely sensed~~ remotely sensed ocean color (OC), measured as reflectance, to variations in ~~chlorophyll~~ chlorophyll-a concentration (see O'Reilly and Werdell, 2019, for an extensive evaluation of OC ~~band ratio~~ band-ratio algorithms). Because these algorithms perform well, a plethora of studies have been conducted based on ~~those them~~, notably about phytoplankton phenology (e.g., Vargas et al., 2009) and phytoplankton primary production (see Carr et al., 2006, and references therein).

~~Space-borne~~ Spaceborne monitoring of aquatic ecosystems is more challenging for optically complex ~~Case-2~~ Case-2 waters (Morel and Prieur, 1977) often found in coastal areas. In contrast to ~~Case-1~~ Case-1 waters, the optical properties of ~~Case-2~~ Case-2 waters are determined by several types of constituents occurring in individually highly variable concentrations. Rivers draining large catchment areas deliver important quantities of optically significant substances such as chromophoric dissolved organic matter (CDOM) and suspended particulate matter (SPM) to the coastal waters (Hedges et al., 1997; Cole et al., 2007; Massicotte et al., 2017). In shallow areas, bottom reflectance and resuspension of sediments can also alter the signal of water-leaving reflectance (Lee et al., 1998). Because CDOM and SPM do not necessarily ~~covary~~ co-vary with chlorophyll *a* and can mask the ~~presence~~ presence ~~CE4~~ of phytoplankton (Sathyendranath, 2000), bio-optical algorithms developed for ~~Case-1~~ Case-1 waters are generally not appropriate for ~~optically-complex~~ Case-2 ~~optically complex~~ Case-2 waters (Gordon and Morel, 1983). Hence, concomitant in situ measurements of optically active components (CDOM, SPM, or chlorophyll *a*) and related radiometric ~~quantities~~ quantities (AOPs and IOPs) are, to this day, critically needed to develop and improve bio-optical algorithms for coastal areas.

The objective of the Coastal Surveillance Through Observation of Ocean Color (COASTℓOOC) oceanographic expeditions was to acquire a comprehensive set of AOPs, IOPs, and concentrations of optically significant components along ~~the~~ European coasts to help the development of new ~~remote sensing~~ remote-sensing algorithms in optically complex waters. Back in 1997 and 1998, the COASTℓOOC campaigns were among the very first concerted efforts to fill the knowledge gaps in coastal marine optics by establishing a large, consistent, and comprehensive optical dataset for coastal waters. A total of 379 stations were visited along the coasts of the Mediterranean, Adriatic, Baltic and Sea, Adriatic Sea, Baltic Sea, North Sea, in the English Channel, and in the Atlantic Ocean, mostly in coastal, ~~but also in open oceanic~~ but also open-ocean waters. While this unique set of data has been used or referenced over the years in numerous peer-reviewed publications (see the list in Appendix A), a reference final dataset, with well-documented quality controls, has never been published. Even though the COASTℓOOC campaigns were carried out more than 20 years ago, the rich and historical dataset that has been collected still has great potential to contribute to the development and evaluation of new bio-optical models adapted for ~~optically-complex~~ optically complex waters. The goal of this paper is to formally present a quality-controlled and final reference version of the COASTℓOOC dataset, ~~archived~~ in a public repository where users can download it readily.

2 Study area and sampling overview

2.1 Study area and general sampling strategy

During the six COASTℓOOC campaigns, further referred to as C1 to C6, a total of 379 locations were visited (Fig. 1). The stations were located along the coasts of the Gulf of Lion in the Mediterranean Sea ($n = 61$), the Adriatic Sea ($n = 39$), the Baltic Sea ($n = 57$), the North Sea ($n = 99$), the English Channel ($n = 85$) ~~and~~, and ~~the~~ Atlantic Ocean ($n = 38$). Within each area, the stations were generally distributed along across-shore or along-shore transects to capture the land-to-sea gradients and document river plumes (Fig. 1b). COASTℓOOC campaigns were either ship-based (C1, C4, C5) or used a helicopter as a sampling platform (C2, C3, C6) and took place between 2 April 1997 and 25 September 1998 (Fig. 2a). Compared to traditional ship-based sampling, the helicopter platform allowed efficient stations close to the coast in areas difficult to access by boat (some samples were collected in waters as shallow as 1 m, Babin, 2003). Combining both ship and airborne sampling approaches allowed ~~covering~~ the whole inshore to open-ocean aquatic continuum ~~to be covered~~. The bathymetry (GEBCO Bathymetric Compilation Group 2021, 2021) varied greatly across the stations, where it averaged ca. 10 m in the Adriatic Sea and ca. 800 m in the ~~Case-1~~ Case-1 Atlantic Ocean (Fig. 2b).

2.2 Water sampling and processing

On board the ship, water samples were analyzed and/or stored immediately after collection. When using a helicopter as a sampling platform, water samples were kept in polyethylene containers for no longer than ~~two hours~~ 2 h after sampling (see Babin, 2003, for further details). Filtration was conducted at low vacuum onto 25 mm ~~glass fiber~~ glass-fiber filters (Whatman, GF/F) to collect particles for subsequent analyses, as described below. Three separate subsamples (up to ~~two liters~~ 2 L each) were filtered for each sample with the following purposes. To determine the concentration of ~~suspended particulate matter (SPM)~~ SPM (g m^{-3}), the particles collected onto a pre-weighed GF/F filter were dried and stored in a freezer at -80°C until the dry weight was determined less than ~~two~~ 2 months later in the laboratory (Van Der Linde, 1998). For pigment analysis, the filter with collected particles was inserted into a cryotube and kept in liquid nitrogen until analysis less than ~~three~~ 3 months later. High-performance liquid chromatography (HPLC) was used as described by Vidussi et al., 1996 (Vidussi et al., 1996) to determine liposoluble pigment concentrations. Total chlorophyll *a* is ~~here defined~~ defined here as the sum of chlorophyll *a*, divinyl chlorophyll ~~divinyl chlorophyll~~ *a*, chlorophyll ~~chlorophyll-a~~ isomer and epimer, chlorophyllids *a*, ~~and phaeopigments~~ CES, and ~~pheopigments~~. The concentrations of particulate organic carbon and nitrogen (POC and PON, respectively) were determined us-

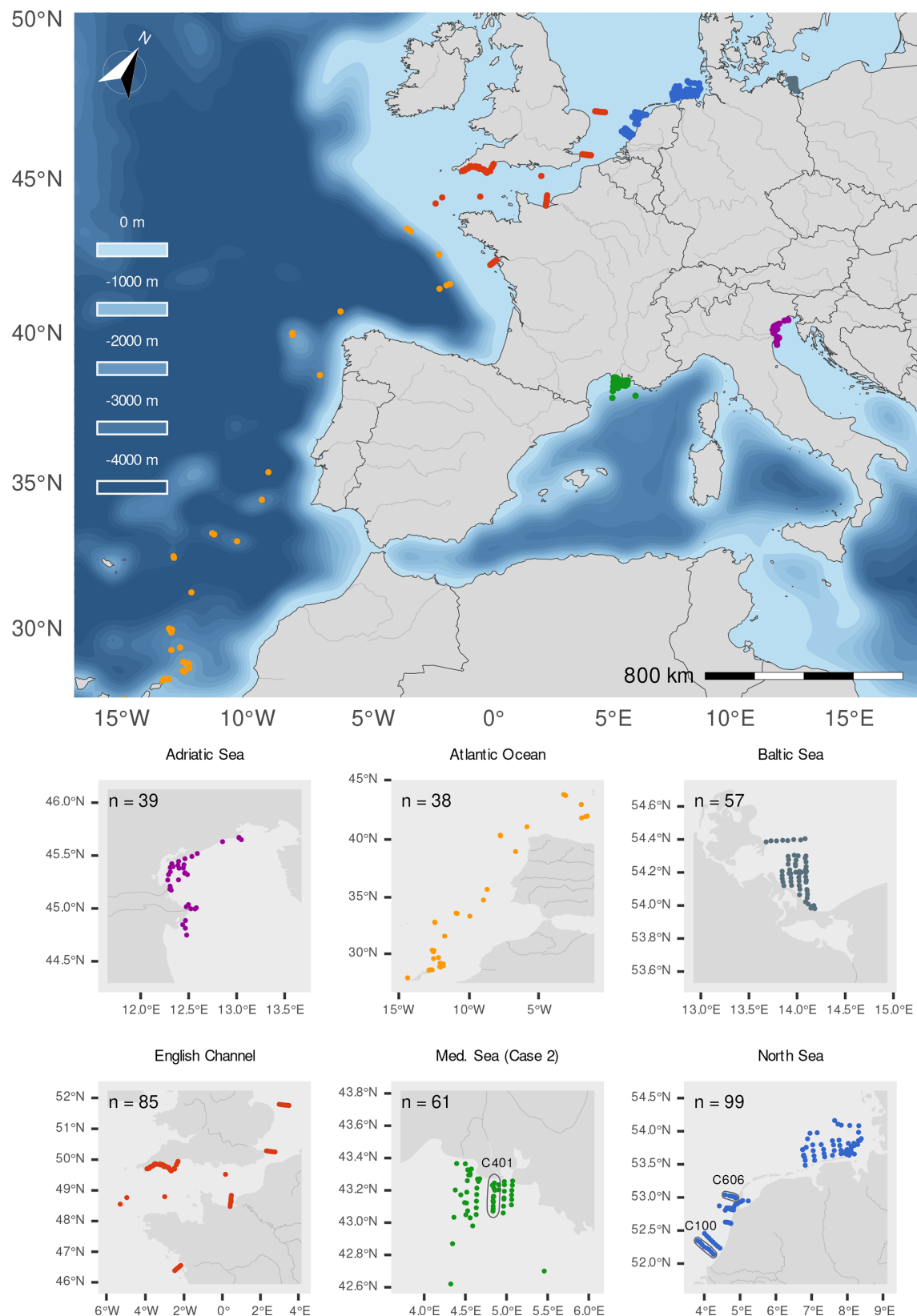


Figure 1. Map of the sampling stations. The three black outlines in the bottom panels (Mediterranean Sea and North Sea) identify the stations and the transects used in Fig. 5e (C100) as well as for the examples of vertical profiles of $K_{\text{Ed}}(490)$ in Fig. 8 (C401 and C606).

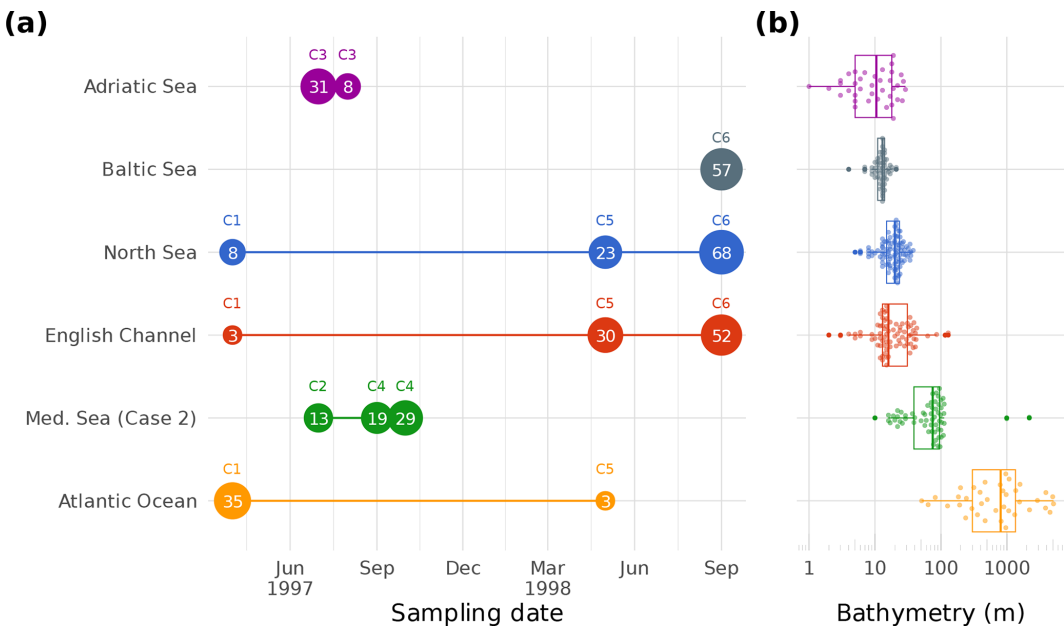


Figure 2. (a) Overview of the temporal sampling for the six areas. The numbers in the circles indicate the number of visited stations each month. (b) Boxplot showing the bathymetry at the sampling locations by area. The labels on top of each circle identify the COASTℓOOC campaigns (C1 to C6).[TS1](#)

ing a Carlo Erba NCS 2500 elemental analyzer as described in Ferrari et al., 2003[Ferrari et al. \(2003\)](#). These determinations were made on particles collected on a GF/F filter precombusted at 450 °C for 2 h and stored in the freezer at –80 °C until analysis less than ~~two~~[two](#) months later. Further details concerning laboratory analyses can be found in Babin, 2003; Ferrari, 2000; Ferrari et al., 2003[Babin \(2003\)](#), Ferrari (2000), and Ferrari et al. (2003). To determine the concentration of dissolved organic matter~~CE6~~[\(DOC, MCE7\)](#), seawater samples were filtered on a 0.22 mm Millipore membrane. The final filtrate was transferred to a 100 mL amber-glass bottle, stored in the refrigerator, and analyzed within ~~three~~[three](#) weeks. DOC was determined by high-temperature catalytic oxidation using a Carlo Erba 480 analyzer. The methodological details can be found in Ferrari, 2000[Ferrari \(2000\)](#).

2.3 Optical measurements

At each station, an optical package was deployed in the water column from the surface, down to ~~one~~[one](#) to 2 m above the ocean bottom in shallow waters, and to maximum depths of ca. 100 m in deep waters. The package included a CTD (conductivity, temperature, and depth) as well as and an array of optical instruments to simultaneously measure beam attenuation, absorption and scattering coefficients, as well as irradiance in the water column. The Modular Data and Power System (MODAPS) data-gathering system from Wet-labs Inc., USA, was used to combine the time-stamped data from the different instruments to produce a data matrix with

a common depth grid. For further information, please refer to the COASTℓOOC final report (Aiken et al., 2000).

A specific aspect of COASTℓOOC is the use of a helicopter as a sampling platform, which has enabled high-frequency visiting of sites in very shallow waters (see Sect. 2.1). An additional advantage is due to the fact that helicopter-based optical measurements are not influenced by the sampling platform itself, unlike ship-based measurements unavoidably affected by the presence of the ship's hull, most prominently close to the surface. A drawback of this approach is the difficulty to operate in operating a helicopter stationary at a constant height, especially at under low or gusty wind conditions: while the former requires substantial flight heights to avoid prevent the helicopter downdraft from impacting the optical measurements, rendering sampling less efficient, the latter can result in unwanted vertical movements of the instrument package in water on the order of 1–2 m s⁻¹. To ensure the availability of data of sufficient quality close to the surface, several consecutive up-upcasts and downcasts were therefore performed at each “helicopter” site. Among the measured vertical profiles at each site, the most suitable casts for depth merging and surface extrapolation (which are not necessarily the same;[;](#) see the end of Sect. 2.3.3) were selected using a combination of objective criteria and visual inspection.

2.3.1 Irradiance measurements

The SeaWiFS Profiling Multichannel Radiometer (SPMR, Satlantic Inc., Canada) was used to measure downward (E_d)

and upward (E_u) spectral irradiances ($\text{W m}^{-2} \mu\text{m}^{-1}$) in the water column. Irradiance was measured at 13 wavelengths matching the MERISCE8 channels of direct relevance for ocean observations (411, 443, 456, 490, 509, 531, 559, 619, 664, 683, 706, 779, and 866 nm, except for COASTℓOOC 1 operating at 590 nm instead of 619 nm), ranging from the blue part of the spectrum to the near-infrared at an acquisition rate of 6 Hz. The actual wavelengths differ slightly between upward and downward observations.

The SPMR was fixed to the IOP instrument frame, except for the COASTℓOOC 5 mission, where it was used in free-falling mode. For the ship-based measurements, concomitant observations of the in-air downward spectral irradiance at the sea surface were performed to account for changes in the incoming solar radiation during the in situ profiling (e.g., due to clouds). This approach was not achievable for the helicopter-based measurements, since there was no suitable place to mount the radiometer. For these campaigns, measurements of E_d taken made by the profiler while in the air (i.e., before and after the in-water measurements) were used to assess E_d on the sea surface. In order to minimize the time lag between the in-water measurements and the E_d values on the sea surface, our processing code automatically chose the air measurements closest in time. Under stable atmospheric conditions, no significant error is expected to result from this approach, while it will contribute to increased variability in the retrieved parameters when sampling under varying cloud cover. However, the practical impact of this is limited due to the short duration of helicopter-based sampling, typically lasting between one and three minutes 1 and 3 min per profile.

2.3.2 Water-leaving reflectance

To calculate the water-leaving reflectance, accurate measurements of both E_d and E_u just below the water surface ($z = 0^-$) are needed. In case no spectrally matching in-air E_d reference data are available (as is the case for the helicopter-based campaigns), this was done by extrapolating both $E_d(z)$ and $E_u(z)$ vertical profiles toward the sea surface by fitting an exponential model for the depth dependence of the measured spectral irradiance values (Eq. 1):

$$\Gamma(\lambda, z) = \Gamma(\lambda, 0^-) e^{-K_\Gamma(\lambda)z}, \quad (1)$$

where $\Gamma(\lambda, z)$ is either E_d or E_u measured at wavelength λ and at depth z , $\Gamma(\lambda, 0^-)$ is E_d or E_u estimated just below the air-water interfaceair–water interface, and K_Γ is the estimated diffuse attenuation coefficient for downward (K_{E_d} , m^{-1}) or upward (K_{E_u} , m^{-1}) irradiance. Note that a correction to account for instrument self-shading of the upwelling irradiance was not applied. We assume that the impact of this omission is relatively small except for highly absorbing waters (depending on constituent concentration and/or observation wavelength), where it may lead to an underestimation of near-surface upwelling irradiances.

In case concomitant spectrally matching in-air $E_d(0^+)$ reference data are available (as is the case for most ship-based campaigns), $E_d(0^-)$ is calculated from $E_d(0^+)$ by applying a constant factor of 0.943 to account for losses of the downwelling irradiance (direct + diffuse) due to Fresnel reflection at the rough sea surface. The derived $E_u(0^-)$ and $E_d(0^-)$ values were thereafter used to calculate the water reflectance $R(0^+)$ just below the sea surface:

$$R(0^-) = \frac{E_u(0^-)}{E_d(0^-)}. \quad (2)$$

Vertical irradiance profiles in the red and near-infrared channels at wavelengths beyond 600 nm were fitted using a sum of two exponential functions, of which one represents the diffuse attenuation due to absorption and elastic scattering for the channel under consideration, while the other accounts for Raman scattering from the corresponding (shorter) excitation wavelengths significantly contributing to the upward light field (e.g., Sugihara et al., 1984). Not doing so, i.e., using just a single exponential function, leads to substantial underestimation of the extrapolated subsurface values due to significant Raman contribution contributions from excitation wavelengths with significantly lower K values (see Appendix A). Figure A1 showing the near-surface depth dependence of E_u at 779 nm demonstrates why the two-function approach is required. Below a depth of ca. 1.5 m, the signal is strongly dominated by Raman scattering and is therefore characterized by a diffuse attenuation coefficient very close to that of the corresponding excitation wavelengths.

2.3.3 Irradiance depth merging

Depth-merged irradiance profiles were derived for all the sites by applying a standardized approach. The underlying strategy for depth merging was to provide users with the information they need to do their analyses while modifying the original data as little as possible. Processing was therefore limited to procedures that could be applied equally to all COASTℓOOC campaigns, whether helicopter- or ship-based. For example, variations of the incoming solar radiation were not considered in the depth merging process, since such observations were not available for the helicopter-based campaigns. However, if measured while operating from research vessels, such information is included in the depth-merged profile data to allow users doing to do their own subsequent analyses.

Typically, several upcast and downcast vertical profiles were performed, especially when using the helicopter as a sampling platform, to increase the potential availability of high-quality observations. The actual merging process was executed as follows. First, any observation not meeting both of the two following conditions was discarded: (1) SPMR instrument tilt smaller than 20° and (2) SPMR vertical speed between 0.1 and 2.0 m s^{-1} . To automatically

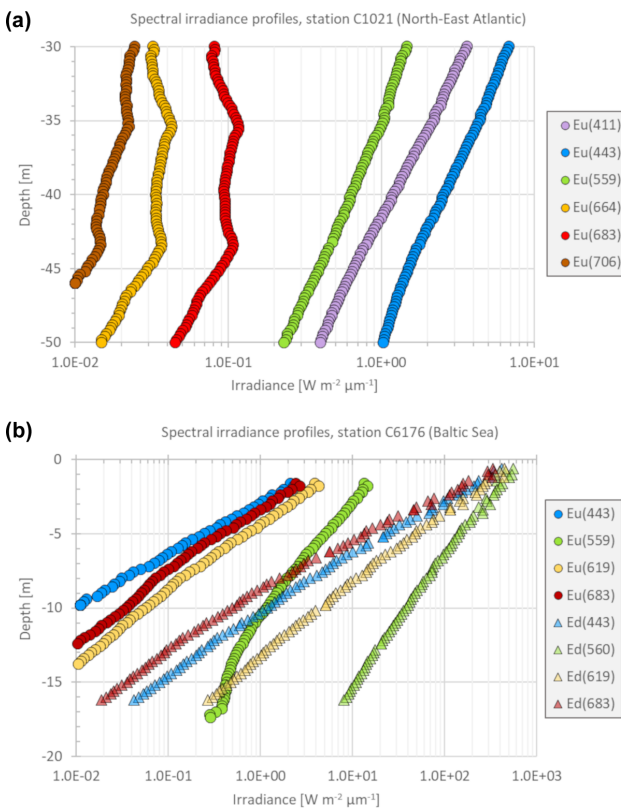


Figure 3. (a) Vertical profile of the upwelling irradiance taken on 11 April 1997 at station C1021 located in the North-East Atlantic offshore Northern-of northern Portugal. (b) Vertical profiles of the upwelling and downwelling irradiance taken on 25 September 1998 at station C6176 located in the Baltic Sea offshore of Usedom Island in North-East Germany. See the text for further details.

identify the best-suited cast for profile generation, the observations meeting fulfilling the above two conditions were then distributed cast-wise over 0.2 m wide vertical bins, starting at zero depth. Finally, the cast with the highest number of bins containing at least one valid observation was selected for depth profile generation, if it fulfilled two further conditions: (3) at least 2 m vertical distance between the highest and the lowest bin lowest bins and (4) at least 50 % of the bins containing at least one observation. No depth merged data is provided for stations where there is no cast meeting fulfilling all of the above four conditions. Combining several casts taken at one station has not proven successful due to potentially large discontinuities in the aggregated values at depth levels where the number of available casts changes, especially in under unstable atmospheric conditions with the corresponding short-term irradiance fluctuations.

Actual depth merging was done by taking the median of all the observations of a particular irradiance parameter within each depth bin. Spectral irradiance observations were only

considered for values above $0.01 \text{ W m}^{-2} \mu\text{m}^{-1}$ to reduce the impact of residual dark current and radiometric noise. Finally, an attempt was made to identify and mask out remaining outliers in the depth-merged irradiance profiles. This was done by applying Grubb's test at a 5 % significance level (Guthrie, 2012) to the residual of a second-order polynomial fit of the logarithmic-transformed spectral irradiance observations for a 2 m depth window, sliding down in steps of 1 m. While this procedure has successfully identified individual spikes, some obvious outliers extending over several depth bins remain in the merged dataset, and users will need to make their own judgment on how to identify and remove those.

Examples of depth-merged irradiance profiles are shown in Fig. 3 for one clear-water site in the NE Atlantic (Fig. 3a) and one CDOM-rich site in the Baltic Sea (Fig. 3b). Figure 3A-a features a double deep chlorophyll maximum with the corresponding irradiance increase due to chlorophyll fluorescence at water depths between ca. 35 and 45 m, most prominently visible at 683 nm, but also affecting the neighboring channels at 664 and 706 nm. Diffuse attenuation in the blue to green wavelengths is correspondingly enhanced, as reflected by the change in slope at a depth of ca. 34 m. Figure 3b features Baltic Sea waters rich in CDOM, resulting in strong absorption in the UV and blue parts of the spectrum. The reduced decrease in the upwelling irradiance at 559 nm towards toward larger depths is likely caused by the reflection of downwelling irradiance from the ocean bottom, while chlorophyll fluorescence is likely the reason for the relatively enhanced (change in slope) upwelling irradiance at 683 nm for depths below ca. 7 m.

Note that extrapolated surface values and depth-merged profiles for a specific site are not necessarily derived from the same observations. This is especially true for helicopter-based operations typically comprising several up-and downcast upcasts and downcasts close to the water surface to increase the likelihood of having sufficient observations for the surface extrapolation, while usually only one or two deep-water casts were made to obtain observations at greater depth. The best-suited observations for surface extrapolation, therefore, do not necessarily correspond to the cast used for depth merging.

2.3.4 Profiles of the diffuse attenuation coefficient

Downward (K_{E_d} , m^{-1}) and upward (K_{E_u} , m^{-1}) spectral diffuse attenuation coefficients have been derived from the depth-merged irradiance data by fitting an exponential function through the irradiance observations within a 2 m depth window, sliding down in steps of 0.2 m. The calculation was only performed if at least five observations were available for fitting within the depth window. The choice of the window width was based on a compromise between two conflicting requirements: on the one hand, it should be

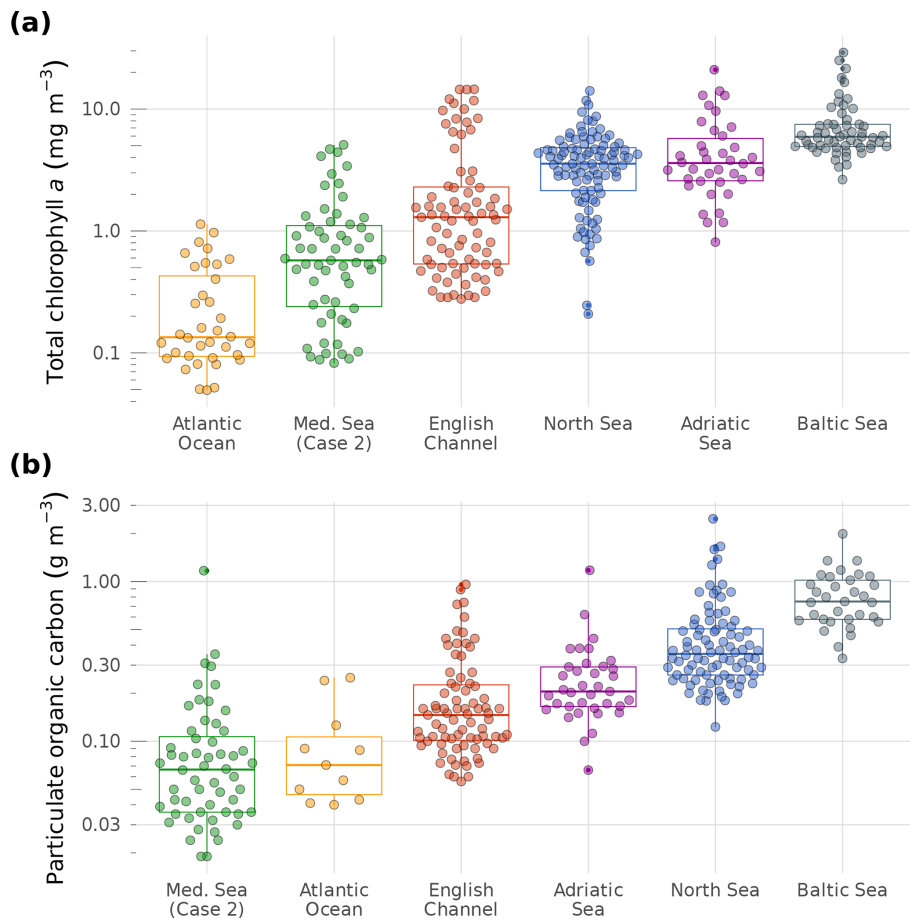


Figure 4. (a) Total chlorophyll a and (b) particulate organic carbon across the sampled areas.

small enough to allow resolution of relatively narrow vertical features, such as a deep chlorophyll maximum. On the other hand, it should be large enough to allow for an accurate estimation of K . The window width of 2 m chosen herein favors vertical resolution over accuracy: while even relatively narrow vertical features remain distinguishable in the derived their own derived K profiles, these are on the other hand affected by remaining outliers, instrument tilt variations, or instrumental noise. Obviously, users may use depth-merged irradiance profiles to derive K profiles or depth-integrated K values better meeting that better meet individual requirements.

2.3.5 Chromophoric dissolved organic matter (laboratory measurements)

Measurements of chromophoric dissolved organic matter (CDOM) absorption (a_{CDOM} , m^{-1}) were performed in the laboratory using a spectrophotometer (Perkin Elmer, Lambda 12) on water samples (10 cm cuvette path length) filtered on a $0.22\ \mu m$ Millipore membrane pre-rinsed with 50 mL of Milli-Q water (Babin, 2003). a_{CDOM} spectra

were measured between either 300–750 or 350–750 nm at a 1 nm increment.

2.3.6 Particulate, non-algal, and phytoplankton absorption (laboratory measurements)

Water samples were filtered onto 25 mm glass-fiber filters (Whatman, GF/F) at a low vacuum before absorption measurement (Babin, 2003). Total particulate absorption (a_p , m^{-1}) was measured on particles retained on the filters between 380 and 750 nm at a 1 nm increment using a spectrophotometer equipped with a 60 mm integrating sphere (Perkin Elmer, Lambda 19) and following the transmittance-reflectance-transmittance-reflectance (TR) method (Tassan and Ferrari, 1995, 1998). Afterward, pigments were removed from the particles with sodium hypochlorite to measure non-algal (or non-pigmented) absorption (a_{NAP} , m^{-1}). Finally, phytoplankton absorption (a_ϕ , m^{-1}) was retrieved by subtracting a_{NAP} from a_p . a_{CDOM} and a_{NAP} absorption spectra were fitted according to the following equation (Jerlov,

1968; Bricaud et al., 1981):

$$a_\tau(\lambda) = a_\tau(\lambda_0)e^{-S_\tau(\lambda-\lambda_0)} + k, \quad (3)$$

Where *where* a_τ is the absorption coefficient, either a_{CDOM} or a_{NAP} (m^{-1}), λ is the wavelength (nm), λ_0 is a reference wavelength (443 nm), S_τ is the spectral slope (nm^{-1}) that describes the approximate exponential decrease in absorption with increasing wavelength, and k is a background constant (m^{-1}) accounting for scatter in the cuvette and drift of the instrument. a_{CDOM} spectra were fitted using observations below 700 nm, whereas a_{NAP} fits were performed between 380 and 730 nm, excluding spectral regions between 400–480 and 620–710 nm to avoid possible residual pigment absorption (Babin, 2003). a_{CDOM} and a_{NAP} were baseline-corrected by subtracting the background parameter (k) derived from the following equation:

$$\hat{a}_\tau(\lambda) = a_\tau(\lambda) - k. \quad (4)$$

Finally, the spectral background of a_P spectra (i.e., the average absorption measured between 746 and 750 nm) was added to a_{NAP} . The underlying rationale is that absorption by phytoplankton in the near-infrared (NIR) is null, and that absorption measured in the NIR for total particles using the TR method is real (Tassan and Ferrari, 2003) and belongs exclusively to non-algal particles. The absorption signal measured for total particles retained on untreated filters is assumed to be more reliable than that measurement on bleached filters.

2.3.7 Total absorption and scattering (in situ measurements)

In situ vertical profiles of absorption (a , m^{-1}) and beam attenuation (c , m^{-1}) were acquired at nine wavelengths (412, 440, 488, 510, 555, 630, 532 or 650 depending on the instrument configuration, 676, and 715 nm) using a flow-through in situ absorbance-attenuance-absorbance-attenuance meter (AC9, Wetlabs). As the measurements are referenced to pure (Milli-Q) water, the obtained absorption and attenuation coefficients exclude the contribution of water. To correct absorption measurements for incomplete recovery of scattered light, $a(715)$ was subtracted from $a(\lambda \leq 715)$. Scattering coefficients (b , m^{-1}) were calculated by subtracting absorption from attenuation. As the contribution of molecular (water) scattering is excluded (see above), this coefficient essentially corresponds to particle scattering and is hereafter denoted by b_p (m^{-1}).

The such-derived values for a , b_p , and c derived in this way were subsequently averaged over the first attenuation length ($1/K_{E_d}$) to provide values representative of the surface layer. Due to practical difficulties when operating the AC-9-AC9 from a helicopter (e.g., trapped air in the instrument), the availability of a , b_p , and c values is limited for helicopter-based campaigns, especially

for COASTIOOC COASTℓOOC 3 (Adriatic Sea). Surface-to-bottom depth merging of the full AC-9-AC9 profiles has not been attempted so far, but this is envisaged for a potential future reprocessing of the COASTℓOOC dataset (see Sect. 5).

55

3 Data quality control and data processing

Different general quality-control procedures were adopted to ensure the integrity of the data. First, the raw data were visualized and screened to eliminate errors both originating from the measurement devices, including sensors (systematic or random), and errors inherent to measurement procedures and methods. Statistical metrics such as average, standard deviation, and range were computed to detect and remove anomalous values in the data. Then, data were checked for duplicates and remaining outliers. The complete list of variables is presented in Table 1.

60

65

70

75

80

85

90

95

4 Data description (an overview)

4.1 Spatial variability along the coastal-ocean gradient

The COASTℓOOC sampling strategy was primarily designed to capture the bio-optical gradient across the sampled ecosystems and along transects from the coast towards the open ocean within each area (Fig. 1). The following sections present an overview of a few selected variables measured in the different areas. An extensive and detailed explanatory visualization analysis is presented in the final report of the COASTℓOOC project (Aiken et al., 2000).

4.1.1 Chlorophyll *a* and particulate organic carbon

As observed in Fig. 4, both total chlorophyll-*a* and particulate organic carbon (POC) concentrations varied markedly across the sampled areas, reflecting the natural gradient captured by the sampling strategy. Across all the stations, total chlorophyll *a* ranged between 0.05 and 29 mg m^{-3} . The median chlorophyll *a* ranged between ca. 0.15 mg m^{-3} in the Atlantic Ocean and 5.9 mg m^{-3} in the Baltic Sea (Fig. 4a). Based on the definition proposed by Antoine et al., 1996 Antoine et al. (1996), the sampled stations were representative of a wide range of trophic status: oligotrophic ($n = 17$, chlorophyll *a* $\leq 0.1 \text{ mg m}^{-3}$), mesotrophic ($n = 106$, $0.1 \leq \text{chlorophyll } a \leq 1 \text{ mg m}^{-3}$), and eutrophic ($n = 245$, chlorophyll *a* $> 1 \text{ mg m}^{-3}$). A similar shore-to-sea gradient pattern could be observed for POC, with median values varying between ca. 0.07 g m^{-3} and 0.8 g m^{-3} in the Mediterranean Sea (easeCase 2) and the Baltic Sea, respectively (Fig. 4b, range between 0.02 and 2.5 g m^{-3}).

Table 1. List of measured parameters.[CE10](#)

| Variable | Units | Source file | Description |
|-----------------------------------|---------------------------|-------------|--|
| Wavelength | nm | 100303.csv | |
| a_p_m1 | m^{-1} | 100303.csv | Total particulate absorption |
| a_nap_m1 | m^{-1} | 100303.csv | Non-algal absorption |
| a_nap_adjusted_m1 | m^{-1} | 100303.csv | Non-algal absorption adjusted so that the baseline background is equal to that of ap CE11 |
| a_cdom_m1 | m^{-1} | 100303.csv | Chromophoric dissolved organic matter absorption |
| a_cdom_adjusted_m1 | m^{-1} | 100303.csv | Chromophoric dissolved organic matter absorption with the background baseline removed |
| a_phy_m1 | m^{-1} | 100303.csv | Phytoplankton absorption |
| background_a_p_m1 | m^{-1} | 100303.csv | Baseline background of total particulate absorption |
| background_a_cdom_m1 | m^{-1} | 100303.csv | Baseline background of chromophoric dissolved organic matter absorption |
| background_a_nap_m1 | m^{-1} | 100303.csv | Baseline background of non-algal absorption |
| a_m1 | m^{-1} | 100304.csv | Total non-water absorption coefficient |
| c_m1 | m^{-1} | 100304.csv | Total non-water attenuation coefficient |
| bp_m1 | m^{-1} | 100304.csv | Particle-scattering coefficient |
| Longitude | Degree decimal | 100305.csv | Longitude of the pixel used to extract the bathymetry |
| Latitude | Degree decimal | 100305.csv | Latitude of the pixel used to extract the bathymetry |
| bathymetry_m | m | 100305.csv | Bathymetry depth at the sampled stations |
| eu_w_m2_um | $W\ m^{-2}\ \mu m^{-1}$ | 100307.csv | Upward irradiance just beneath the water surface (Eu0-) |
| ed_w_m2_um | $W\ m^{-2}\ \mu m^{-1}$ | 100307.csv | Downward irradiance just beneath the water surface (Ed0-) |
| k_eu_m1 | m^{-1} | 100307.csv | Attenuation coefficient for upward irradiance (just beneath the water surface) |
| k_ed_m1 | m^{-1} | 100307.csv | Attenuation coefficient for downward irradiance (just beneath the water surface) |
| measured_reflectance_percent | % | 100309.csv | Surface water reflectance |
| s_cdom_nm1 | nm^{-1} | 100310.csv | Spectral slope that describes the approximate exponential decrease in a_{CDOM} |
| s_nap_nm1 | nm^{-1} | 100310.csv | Spectral slope that describes the approximate exponential decrease in a_{NAP} |
| a_cdom443_m1 | m^{-1} | 100310.csv | Chromophoric dissolved organic matter absorption at 443 nm |
| a_nap443_m1 | m^{-1} | 100310.csv | Non-algal absorption at 443 nm |
| Station | Free text | 100311.csv | Unique ID of the sampled station: this can be used as a unique key to merge the data across other files. |
| Date | YYYY-MM-DD | 100311.csv | Date on which the measurement was made |
| depth_m | m | 100311.csv | Depth at which the measurement was made |
| Longitude | Degree decimal | 100311.csv | Longitude of the sampling station |
| Latitude | Degree decimal | 100311.csv | Latitude of the sampling station |
| Area | Free text | 100311.csv | Region where the measurement was made: one of (1) North Sea, (2) English Channel, (3) Atlantic Ocean, (4) Med. Sea (Case 2), (5) Adriatic Sea, or (6) Baltic Sea |
| System | Free text | 100311.csv | Dominant river system influencing the site |
| gmt_time | Hours decimal | 100311.csv | Representative time of observations at the site in Greenwich mean time (UTC) |
| solar zenith_angle | Degree | 100311.csv | Solar zenith angle |
| chlorophyll_a_mg_m3 | $mg\ m^{-3}$ | 100308.csv | Chlorophyll <i>a</i> |
| chlorophyll_b_mg_m3 | $mg\ m^{-3}$ | 100308.csv | Chlorophyll <i>b</i> |
| chlorophyll_c_mg_m3 | $mg\ m^{-3}$ | 100308.csv | Chlorophyll <i>c</i> |
| pheopigment_mg_m3 | $mg\ m^{-3}$ | 100308.csv | Pheopigment |
| fucoxanthin_mg_m3 | $mg\ m^{-3}$ | 100308.csv | Fucoxanthin |
| hexanoyloxyfucoxanthin_19_mg_m3 | $mg\ m^{-3}$ | 100308.csv | Hexanoyloxyfucoxanthin-19 |
| butanoyloxyfucoxanthin_19_mg_m3 | $mg\ m^{-3}$ | 100308.csv | Butanoyloxyfucoxanthin-19 |
| alloxanthin_mg_m3 | $mg\ m^{-3}$ | 100308.csv | Alloxanthin |
| zeaxanthin_mg_m3 | $mg\ m^{-3}$ | 100308.csv | Zeaxanthin |
| prasixanthin_mg_m3 | $mg\ m^{-3}$ | 100308.csv | Prasixanthin |
| neoxanthin_mg_m3 | $mg\ m^{-3}$ | 100308.csv | Neoxanthin |
| violaxanthin_mg_m3 | $mg\ m^{-3}$ | 100308.csv | Violaxanthin |
| diatoxanthin_mg_m3 | $mg\ m^{-3}$ | 100308.csv | Diatoxanthin |
| diadinoxanthin_mg_m3 | $mg\ m^{-3}$ | 100308.csv | Diadinoxanthin |
| peridinin_mg_m3 | $mg\ m^{-3}$ | 100308.csv | Peridinin |
| carotene_mg_m3 | $mg\ m^{-3}$ | 100308.csv | Carotene |
| lutein_mg_m3 | $mg\ m^{-3}$ | 100308.csv | Lutein |
| suspended_particulate_matter_g_m3 | $g\ m^{-3}$ | 100306.csv | Suspended particulate matter |
| particulate_organic_nitrogen_g_m3 | $g\ m^{-3}$ | 100306.csv | Particulate organic nitrogen |
| total_particulate_carbon_g_m3 | $g\ m^{-3}$ | 100306.csv | Total particulate carbon |
| particulate_organic_carbon_g_m3 | $g\ m^{-3}$ | 100306.csv | Particulate organic carbon |
| dissolved_organic_carbon_g_m3 | $g\ m^{-3}$ | 100306.csv | Dissolved organic carbon |
| Cast | I | 100312.csv | Processed cast number |
| Depth | m | 100312.csv | Depth of the vertical bin, e.g., -1.00 representing the depth bin [-0.90, -1.10 m] |
| TmpWat | °C | 100312.csv | Water temperature |
| Cond | $ms\ cm^{-1}$ | 100312.csv | Conductivity |
| Salin | PSU | 100312.csv | Salinity |
| SigmaT | 1 | 100312.csv | Quantity (no units) to specify the density of seawater |
| TiProf | Degree | 100312.csv | Tilt of the profiling radiometer |
| TiRef | Degree | 100312.csv | Tilt of the reference radiometer |
| VSpeed | ms^{-1} | 100312.csv | Vertical speed |
| Altim | m | 100312.csv | Altimeter sounding of the distance from the ocean ground CE12 |
| N_OBS | 1 | 100312.csv | Number of observations within the depth bin |
| EUnnn | $W\ m^{-2}\ \mu m^{-1}$ | 100312.csv | In-water upwelling irradiance at wavelength nnn |
| EDnnn | $W\ m^{-2}\ \mu m^{-1}$ | 100312.csv | In-water downwelling irradiance at wavelength nnn |
| ERnnn | $W\ m^{-2}\ \mu m^{-1}$ | 100312.csv | In-air downwelling irradiance at wavelength nnn |
| KUnnn | m^{-1} | 100312.csv | Diffuse attenuation at wavelength nnn calculated from the upwelling irradiance |
| KDnnn | m^{-1} | 100312.csv | Diffuse attenuation at wavelength nnn calculated from the downwelling irradiance |
| PAR_ABS | $\mu mol\ m^{-2}\ s^{-1}$ | 100312.csv | Photosynthetically CE13 active radiation (PAR) |
| PAR%SRF | % | 100312.csv | PAR at depth z relative to PAR on the sea surface |
| K_PAR | m^{-1} | 100312.csv | Diffuse attenuation for PAR |

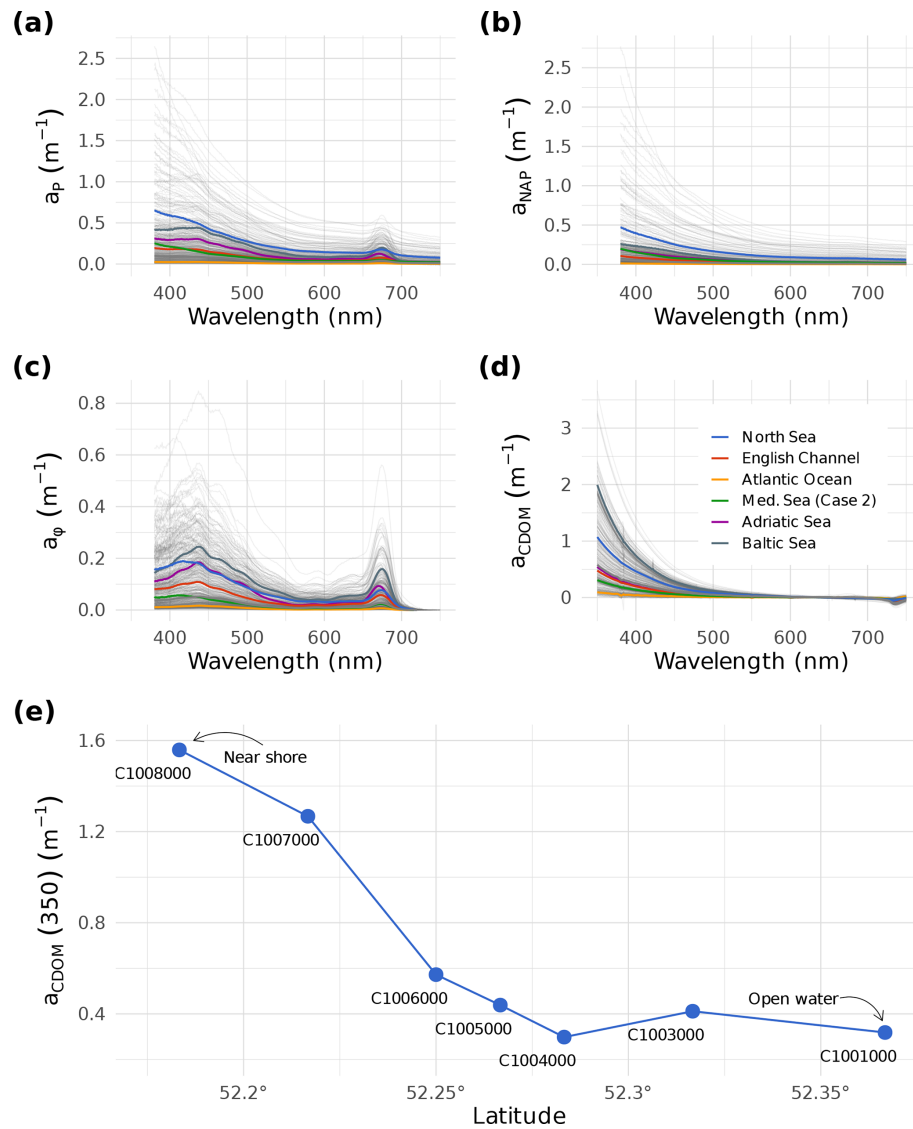


Figure 5. (a) Average total particulate (a_p), (b) non-algal (a_{NAP}), (c) phytoplankton (a_ϕ), and (d) chromophoric dissolved organic matter (a_{CDOM}) absorption spectra in each area. Light gray lines in panels (a–d) show individual absorption spectra measured across the sampled areas. (e) $a_{CDOM}(350)$ along the westernmost transect in the North Sea (see Fig. 1b).

4.1.2 Inherent optical properties (IOPs)

Measured absorption spectra in each area for total particulate (a_p), non-algal particles (a_{NAP}), phytoplankton (a_ϕ), and chromophoric dissolved organic matter (a_{CDOM}) are presented in Fig. 5. Phytoplankton maximum absorption peaks at around 440 and 675 nm are easily distinguishable in Fig. 5c and were found to be highly correlated with the concentration of total chlorophyll *a* (Pearson's $r > 0.90$). Across all the areas, $a_{CDOM}(350)$, a proxy for dissolved carbon concentration, varied between 0.03 and 3.66 m^{-1} . These values fall within the ranges of the mean values reported globally in the ocean (0.14 m^{-1}), coastal (1.82 m^{-1}), and estuarine (4.11 m^{-1}) ecosystems

(Massicotte et al., 2017). Overall, the highest absorption by dissolved organic matter was observed in the Baltic Sea (Fig. 5d). Sampled stations in this area were located ~~West~~ west of the Oder River plume, which drains important quantities of humic substance from its catchment area. In contrast, the lowest CDOM absorption was observed in the Atlantic Ocean, where stations were located away from land and thus less influenced by terrestrial inputs (Fig. 1). The spatial variability of CDOM is further emphasized in Fig. 5e, where $a_{CDOM}(350)$ decreased by a factor of ~~four~~ 4 between the two most distant points (approximately 40 km) of the westernmost transect sampled in the North Sea (see Fig. 1b).

Light scattering by suspended particles in the water column is a driver of reflectance variability and is often used

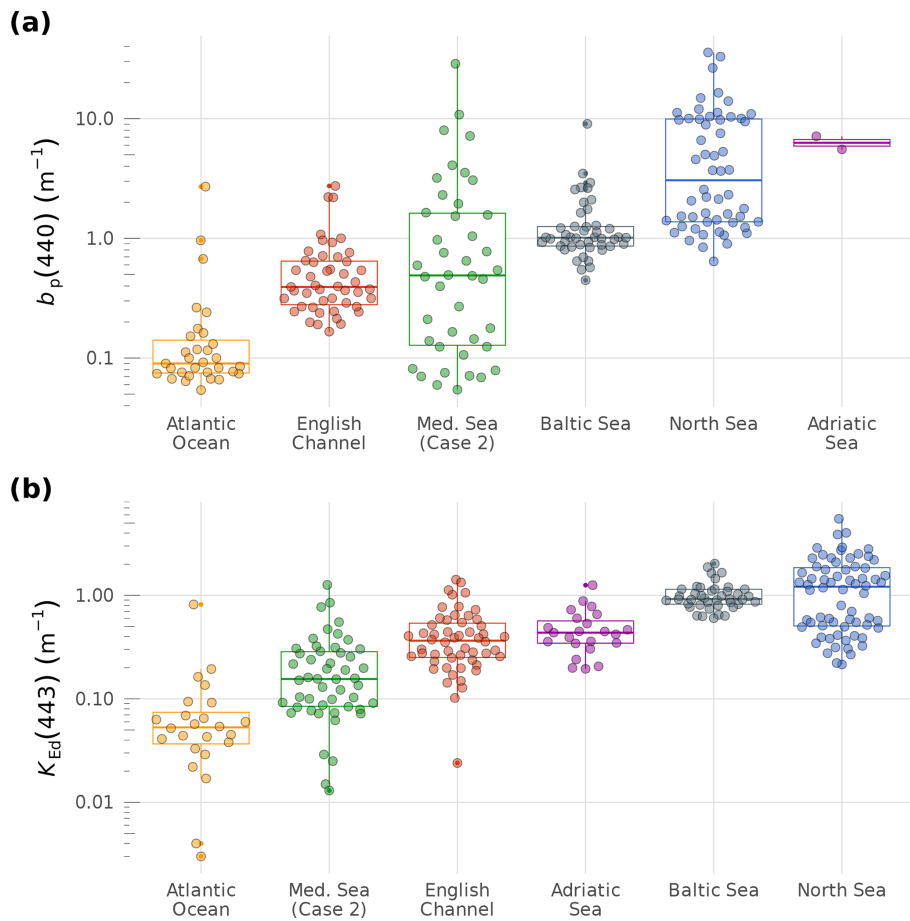


Figure 6. (a) Particulate scattering coefficient at 440 nm ($b_p(440)$) and (b) attenuation coefficient for downward irradiance at 443 nm ($K_{Ed}(443)$) across the sampled areas.

by remote-sensing applications to discriminate between Case-1 and Case-2 waters (Sathyendranath, 2000; Morel and Bélanger, 2006). The particulate scattering coefficient at 440 nm, $b_p(440)$, ranged between 0.05 and 35.8 m^{-1} (Fig. 6a). The median values varied by almost two orders of magnitude between the Atlantic Ocean and the Adriatic Sea (Fig. 6a). Furthermore, $b_p(440)$ showed more or less the same spatial pattern as the downward irradiance attenuation coefficient at 443 nm, $K_{Ed}(443)$, with median $b_p(440)$ values varying between 0.05 and 1.21 m^{-1} in the Atlantic Ocean and the North Sea, respectively (Fig. 6b, Pearson's $r = 0.76$).

4.1.3 Apparent optical properties (AOPs)

Subsurface reflectance $R(0^-)$ – $R(0^+)$ for all COAST ℓ OOC sites is shown in Fig. 7, reflecting the fundamental differences in the bio-optical properties of the different areas visited. For example, due to enhanced CDOM absorption, reflectance in the blue part of the spectrum is generally low at the Baltic Sea sites, while it is higher in the Case-1 waters encountered in the Atlantic Ocean or the Mediterranean Sea.

In the red and NIR, very high reflectance values are observed in the sediment-rich Case-2 waters of the North Sea and the English Channel.

Sample profiles of the diffuse attenuation coefficient $K_{Ed}(490)$ at a vertical resolution between 2.0 m close to the surface and 5.0 m underneath are shown in Fig. 8 for two transition zones ranging from turbid waters close to the coast to clearer waters offshore. Figure 8a shows $K_{Ed}(490)$ values along a transect taken in the Gulf of Lion on 30 September 1997 from site C4014 located ca. 5 km to the west of the mouth of the main Rhône branch (Grand Rhône) to site C4019 some 20 km further south in clear Mediterranean waters. While $K_{Ed}(490)$ at the offshore sites C4017 to C4019 adopts low values between ca. 0.02 and 0.05 m^{-1} reflecting clear-water conditions, sites C4014 and C4015 are strongly influenced by the Rhône river plume, resulting in $K_{Ed}(490)$ reaching values of up to 0.8 m^{-1} in the surface layer. The turbid Rhône freshwater is floating on top of denser and clearer Mediterranean seawater, resulting in a strong stratification. Figure 8b shows a similar transect taken in the North Sea on 12 September 1998 extending from

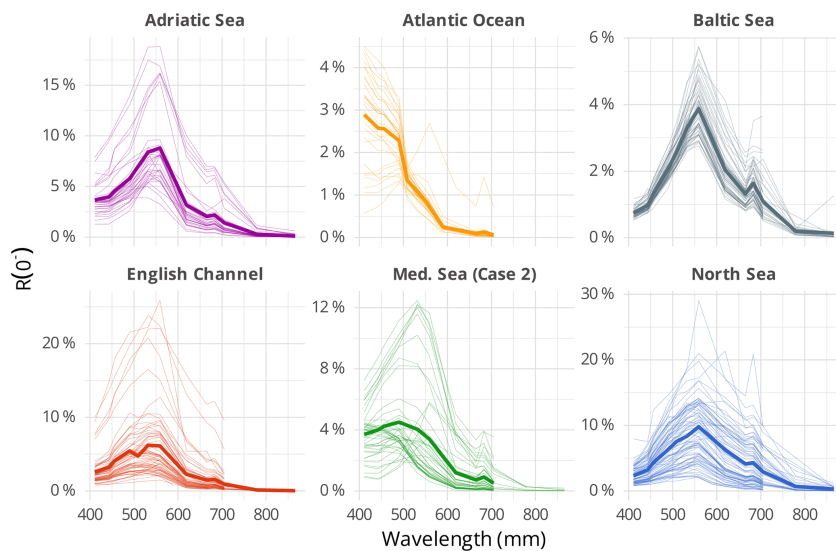


Figure 7. Subsurface reflectance $R(0^-)$ across the sampled areas. The thick lines represent the regional averages. Note that $R(0^-)$ at wavelengths above 705 nm could only be derived from helicopter-based measurements. Please also note that the y-axes are adjusted to the data presented within each subplot.

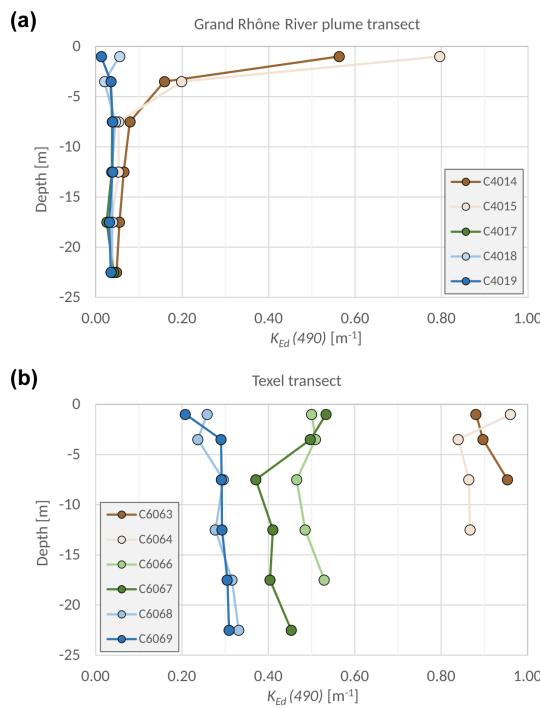


Figure 8. (a) $K_{Ed}(490)$ profiles taken in the Lion's-Gulf of Lion on 30 September 1997 along a transect extending from site C4014 located ca. 5 km to the west of the mouth of the main Rhône branch (Grand Rhône) to site C4019 located some 20 km further south in clear Mediterranean waters. (b) $K_{Ed}(490)$ profiles taken in the North Sea on 12 September 1998 along a transect extending from site C6063 close to the western shore of the island of Texel to site C6069 located ca. 22 km further west in the open North Sea.

site C6063 close to the western shore of Texel island to site C6069 located ca. 22 km further west in the open North Sea. Again, there is a distance-to-coast-dependent decrease of $K_{Ed}(490)$ values likely related to reduced turbidity, from ca. 0.8 to 1.0 m^{-1} close to the coast down to values of ca. 0.2 to 0.3 m^{-1} offshore. In contrast to the transect in the Gulf of Lion, no obvious stratification is observed; $K_{Ed}(490)$ values are rather homogeneously distributed over the entire water column, pointing to effective mixing.

4.2 Co-variability across bio-optical measurements

Few research papers have previously shown how optically significant components and AOPs co-varied during the COASTℓOOC missions (Ferrari, 2000; Ferrari et al., 2003; Babin, 2003; Babin et al., 2003a). In this section, a brief overview of selected pairwise relationships is presented. Total chlorophyll a co-varies with POC (Fig. 4), and the relationship was highly variable (Fig. 9a). Whereas while the global Pearson correlation is 0.79 ($n = 299$), it ranged between 0.36 in the North Sea ($n = 88$) to 0.78 in the Adriatic Sea ($n = 37$), showing that optically significant components do not necessarily co-vary altogether. Likewise, the global Pearson correlation between a_ϕ and total chlorophyll a (Fig. 9b) was relatively high ($r = 0.90$, $n = 338$). The lowest and highest correlations were observed in the North Sea ($r = 0.69$, $n = 88$) and the Adriatic Sea ($r = 0.91$, $n = 38$), respectively. POC concentration is well known to be an important driver of both IOPs and AOPs in aquatic ecosystems (Stramski et al., 2008; Cetinić et al., 2012). Unsurprisingly, positive correlations were observed

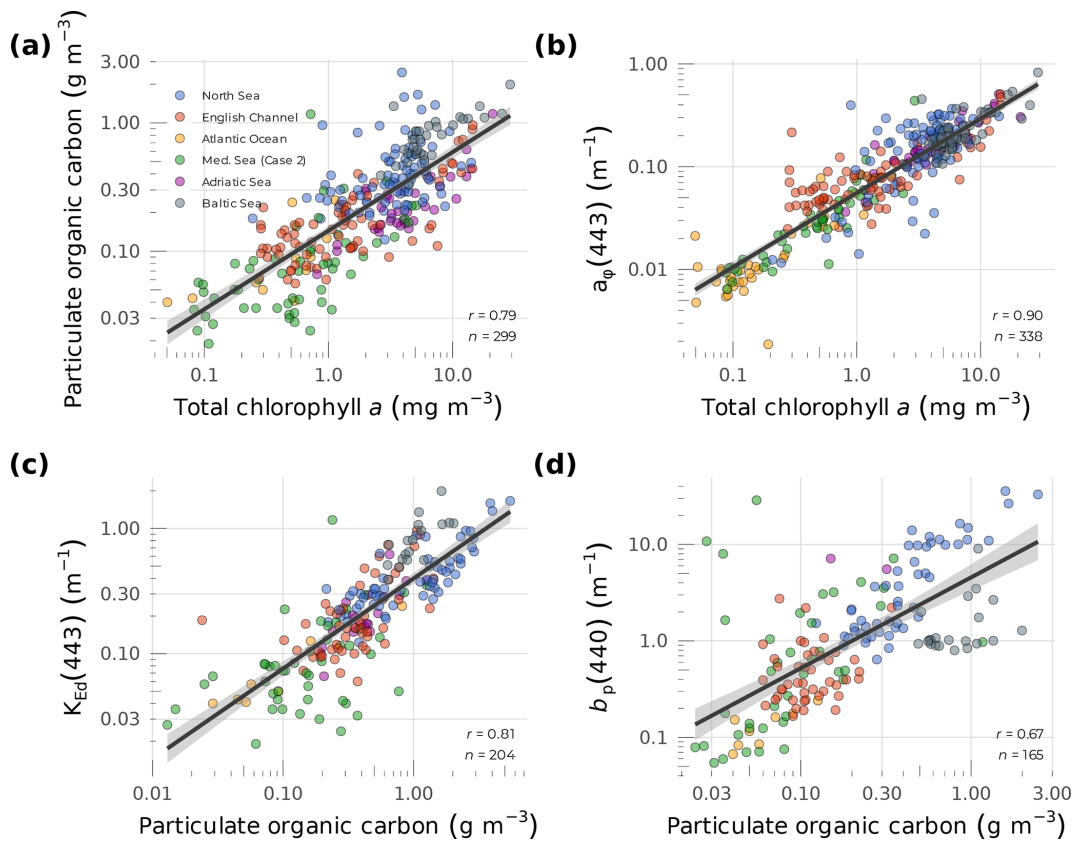


Figure 9. Scatterplots showing relationships among different selected variables. **(a)** Particulate organic carbon (POC) and **(b)** phytoplankton absorption at 443 nm ($a_\phi(443)$) against total chlorophyll a . **(c)** Downward irradiance at 443 nm ($K_{Ed}(443)$) and **(d)** particulate scattering at 440 nm ($b_p(440)$) against particulate organic carbon. The red lines show the linear relationships between the variables. The shaded gray areas represent the 95 % confidence intervals around the fitted models.

between POC and $K_{Ed}(443)$ (Fig. 9c, $r = 0.81, n = 204$) and $b_p(440)$ (Fig. 9d, $r = 0.67, n = 165$).

Based on the size-reactivity-size-reactivity continuum model proposed by Benner and Amon, 2015 Benner and Amon (2015), physicochemical and photochemical processes are shaping shape the size distribution of organic matter along the aquatic continuum, and determine the contrasted intrinsic nature of the particles for each type of ecosystem. This is likely one key reason explaining why the observed relationships are quite variable across the different sampled ecosystems (Fig. 9). For example, in coastal areas (e.g., the Baltic Sea, Fig. 1), the POC content is generally influenced by large humic organic particles drained by rivers from the surrounding watershed (Babin et al., 2003a). Consequently, in these areas, POC concentration (Fig. 4b), absorption (Fig. 5), and downward attenuation coefficients (Fig. 9c) were higher than in other sampled areas. In contrast, the stations that were farther away from the coast (such as the Atlantic Sea, Fig. 1) had lower POC concentrations (Fig. 4b) and absorption (Fig. 5).

Code and data availability. The COASTℓOOC data is provided as a collection of comma-separated values-value (CSV, csv) files that are regrouping regroup measurements associated with each measurement. The processed and tidied version of the data is hosted at SEANOE (SEA scieNtific Open data Edition) under the CC-BY license (<https://doi.org/10.17882/93570>, Massicotte et al., 2023). To aid the user to merge in merging these files, there is a lookup table file designated station list (<https://www.seanoe.org/data/00824/93570/data/100311.csv>) that can serve as a table to join the data together based on the station's unique identifier. Table 1 shows the complete list of available measurements. Please note that the actual filenames (e.g., /100311.csv) are assigned by SEANOE during the upload process and cannot be altered. All statistical analyses were performed in R version 4.3.0 (R Core Team, 2023). The code used to produce the figures and the analysis presented in this paper is available under the GNUCE14 GPLv3 license (<https://doi.org/10.5281/zenodo.8091717>, Massicotte, 2023b). Irradiance depth merging was done with an IDLCE15 code available under the Creative Commons Attribution 3.0 Germany license (<https://doi.org/10.5281/zenodo.8096682>, Fell, 2023). Note that there are plans to update and further improve the current data set dataset. More data will likely be recovered from the backup archives, most prominently AC-9-AC9 measurements to derive in situ vertical profiles of a , b_p , and c . Intended improvements to

radiometer processing comprise (not exhaustively) a better ~~dark~~
15 ~~current~~ ~~dark-current~~ correction, the application of a self-shading
correction, a more accurate treatment of the ~~air/sea~~ ~~air-sea~~ transmission
of downward irradiance (E_d), and a closer look at uncertainties.
Any update of the COASTℓOOC dataset will be made publicly
available through SEANOE.

5 Conclusions

20

The consolidated ~~, and~~ quality-controlled ~~, -~~ data collected
during the COASTℓOOC oceanographic expeditions offer,
even if collected more than ~~twenty~~ ~~20~~ years ago, many possi-
bilities ~~to better understand~~ ~~for better understanding~~ the
25 bio-optical dynamics along the land-to-sea gradient where
~~optically complex~~ ~~optically complex~~ water drained from
watersheds ~~mix~~ ~~mixes~~ with seawater. To ~~this~~ date, nearly
40 peer-reviewed studies have made use of the COASTℓOOC
data set ~~to develop~~ ~~remote sensing~~ ~~dataset to develop~~
30 ~~remote-sensing~~ algorithms and to study the optical proper-
ties of seawater across the ~~coastal-to-open-ocean~~ ~~coastal to~~
~~open-ocean~~ gradient (see Table A1). This now consolidated
and easily accessible ~~data set~~ ~~dataset~~ will facilitate future de-
velopment and evaluation of new bio-optical models adapted
35 for ~~optically complex~~ ~~optically complex~~ waters. In this pa-
per, only a subset of variables has been presented. The reader
is referred to Table 1 for a complete list and description of
variables collected during the COASTℓOOC expeditions.

25

30

35

Appendix A

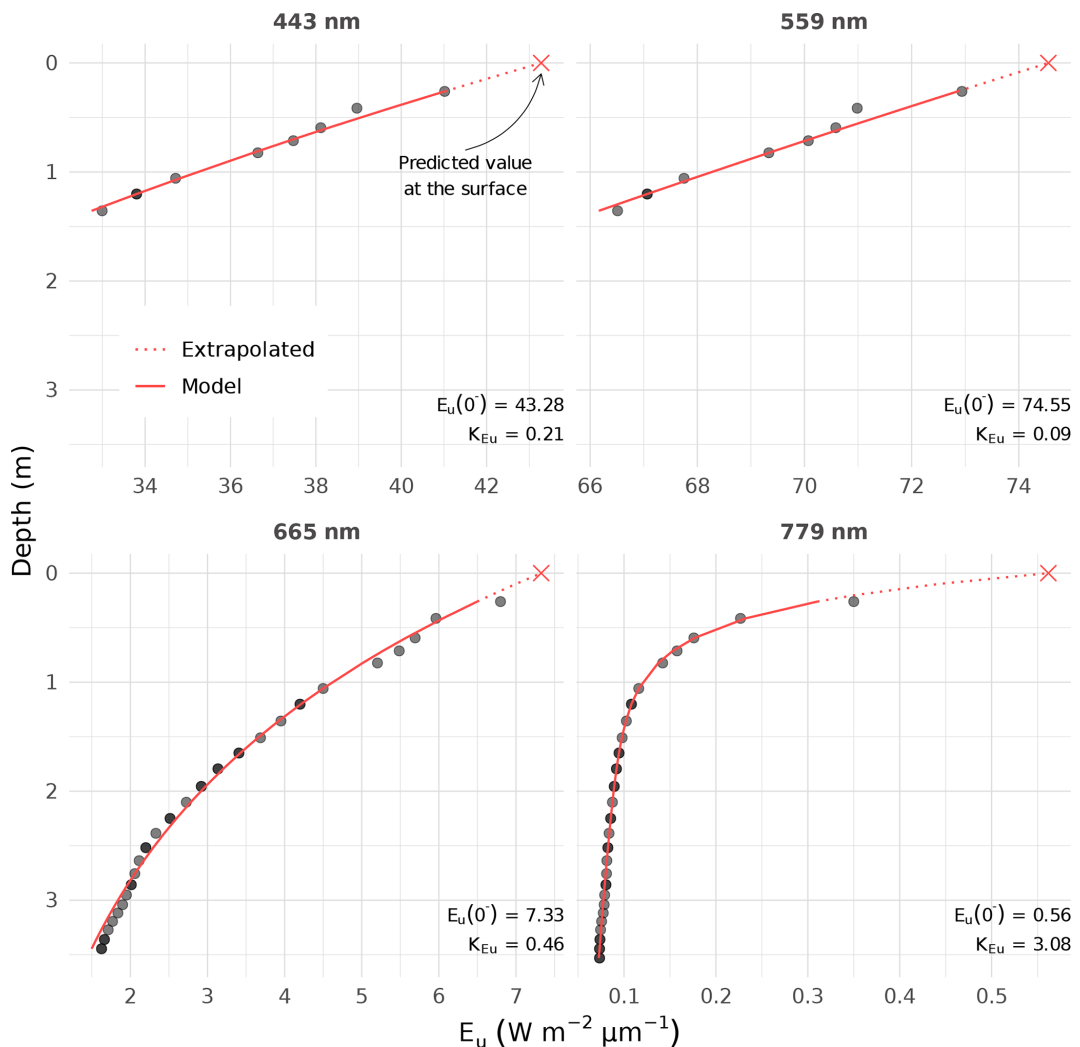


Figure A1. Example of extrapolation of the upward irradiance ~~towards~~ toward the sea surface (station C3004000). The irradiance values just below the sea surface (red crosses, $E_u(0^-)$) and the corresponding diffuse attenuation coefficient for the topmost water layer are specified in the figures. The full lines represent the interpolated values, whereas the dashed lines show extrapolation values up to the sea surface.

Table A1. Scientific articles in peer-reviewed journals using or referencing COASTLOOC COAST ℓ OOC.

Publications TS4

Babin et al. (2023b), Begouen Demeaux and Boss (2022), Belanger et al. (2008), Beltrán-Abaunza et al. (2014), Blix et al. (2019), Caillault et al. (2021), Chami and Platel (2007), Claustre et al. (2000), D'Alimonte et al. (2014), Defoin-Platel and Chami (2007), Doerffer and Schiller (2007), Doron et al. (2007), Doron et al. (2011), Dransfeld et al. (2005), Ferrari (2000), Groom et al. (2009), Jamet et al. (2012), Kratzer and Moore (2018), Loisel et al. (2001), Loisel et al. (2017), Loisel et al. (2018), Matsuoka et al. (2011), Matsuoka et al. (2014), Morel and Bélanger (2006), Neukermans et al. (2012), Oubelkheir et al. (2007), Schroeder et al. (2007), Schroeder et al. (2022), Shahraiyni et al. (2007), Tassan and Ferrari (2002), Tassan et al. (2000), Wei et al. (2021), Yu et al. (2016, 2019), Zhang et al. (2003), Zhang and Fell (2004, 2007), Zheng and Stramski (2013).

Author contributions. Conceptualization: MB. Formal analysis: FF, DD, VFS, MB. Investigation: MB, FF, VFS. Software: DD (AC-9AC9), FF (radiometry), VFS (data acquisition and pre-processing). Writing: PM with support from all the co-authors.

Competing interests. The contact author has declared that none of the authors has any competing interests.

Disclaimer. Publisher's note: Copernicus Publications remains neutral with regard to jurisdictional claims in published maps and institutional affiliations.

Acknowledgements. Many people contributed to the generation of the COAST ℓ OOC database as described herein, be it by contributing to project implementation, supporting field campaigns, performing lab-laboratory work, or providing scientific guidance. In this respect, we would like especially to thank James Aiken, Jean-François Berthon, Annick Bricaud, Hervé Claustre, Roland Doerffer, Giovanni Massimo Ferrari, Hans Hakvoort, Geir Johnsen, Khadija Oubelkheir, Matt Pinkerton, Rainer Reuter, Marcel Wernand, and Grigor Obolensky. We are also grateful to the crews of the ships (NO *Thetis-2*, RV *Poseidon*, and RV *Victor Hensen*) and the helicopter (Commerc'Air SA) we used for collecting the field data.

Review statement. This paper was edited by Giuseppe M. R. Manzella and reviewed by Emmanuel Boss, Jenny Lovell, and David McKee.

References

- .TS5
Aiken, J., Antoine, D., Babin, M., Barth, H., Bricaud, A., Chauton, M., Claustre, H., Doerffer, R., Dowell, M., Fell, F., Ferrari, M., Fischer, J., Fournier-Sicre, Vincent, Hakvoort, H., Hoepffner, N., Johnsen, G., Montagner, F., Moore, G., Morel, A., Obolensky, G., Olbert, C., Pinkerton, M., Reuter, R., Sakshaug, E., and Wernand, M.: COASTLOOC (COAstal Surveillance Through Observation of Ocean Colour) Final Report, Tech. rep., Zenodo, https://doi.org/10.5281/ZENODO.7428384, 2000.
Antoine, D., André, J.-M., and Morel, A.: Oceanic Primary Production: 2. Estimation at Global Scale from Satellite (Coastal Zone Color Scanner) Chlorophyll, Global Biogeochem. Cy., 10, 57–69, https://doi.org/10.1029/95GB02832, 1996.
Babin, M.: Variations in the Light Absorption Coefficients of Phytoplankton, Nonalgal Particles, and Dissolved Organic Matter in Coastal Waters around Europe, J. Geophys. Res., 108, 3211, https://doi.org/10.1029/2001JC000882, 2003.
Babin, M., Morel, A., Fournier-Sicre, V., Fell, F., and Stramski, D.: Light Scattering Properties of Marine Particles in Coastal and Open Ocean Waters Asrelated to the Particle Mass Concentration, Limnol. Oceanogr., 48, 843–859, https://doi.org/10.4319/lo.2003.48.2.0843, 2003a.
Babin, M., Stramski, D., Ferrari, G. M., Claustre, H., Bricaud, A., Obolensky, G., and Hoepffner, N.: Variations in the light absorption coefficients of phytoplankton, nonalgal particles, and dissolved organic matter in coastal waters around Europe, J. Geophys. Res.-Oceans, 108, TS6, 2003b.
Begouen Demeaux, C. and Boss, E.: Validation of Remote-Sensing Algorithms for Diffuse Attenuation of Downward Irradiance Using BGC-Argo Floats, Remote Sens., 14, 4500, TS7, 2022.
Belanger, S., Babin, M., and Larouche, P.: An empirical ocean color algorithm for estimating the contribution of chromophoric dissolved organic matter to total light absorption in optically complex waters, J. Geophys. Res.-Oceans, 113, TS8, 2008.
Beltrán-Abaunza, J. M., Kratzer, S., and Brockmann, C.: Evaluation of MERIS products from Baltic Sea coastal waters rich in CDOM, Ocean Sci., 10, 377–396, https://doi.org/10.5194/os-10-377-2014, 2014.
Benner, R. and Amon, R. M.: The Size-Reactivity Continuum of Major Bioelements in the Ocean, Annu. Rev. Mar. Sci., 7, 185–205, https://doi.org/10.1146/annurev-marine-010213-135126, 2015.
Blix, K., Li, J., Massicotte, P., and Matsuoka, A.: Developing a new machine-learning algorithm for estimating chlorophyll-*a* concentration in optically complex waters: A case study for high northern latitude waters by using Sentinel 3 OLCI, Remote Sens., 11, 2076, TS9, 2019.
Bricaud, A., Morel, A., and Prieur, L.: Absorption by Dissolved Organic Matter of the Sea (Yellow Substance) in the UV and Visible Domains, Limnol. Oceanogr., 26, 43–53, https://doi.org/10.4319/lo.1981.26.1.0043, 1981.
Caillault, K., Roupiez, L., and Viallefond-Robinet, F.: Modelling of the optical signature of oil slicks at sea for the analysis of multi-and hyperspectral VNIR-SWIR images, Optics Express, 29, 18224–18242, 2021.
Carr, M.-E., Friedrichs, M. A., Schmeltz, M., Noguchi Aita, M., Antoine, D., Arrigo, K. R., Asanuma, I., Aumont, O., Barber, R., Behrenfeld, M., Bidigare, R., Buitenhuis, E. T., Campbell, J., Ciotti, A., Dierssen, H., Dowell, M., Dunne, J., Esaias, W., Gentili, B., Gregg, W., Groom, S., Hoepffner, N., Ishizaka, J., Kameda, T., Le Quéré, C., Lohrenz, S., Marra, J., Mélin, F., Moore, K., Morel, A., Reddy, T. E., Ryan, J., Scardi, M., Smyth, T., Turpie, K., Tilstone, G., Waters, K., and Yamanaka, Y.: A Comparison of Global Estimates of Marine Primary Production from Ocean Color, Deep-Sea Res. Pt. II, 53, 741–770, https://doi.org/10.1016/j.dsr2.2006.01.028, 2006.
Cetinić, I., Perry, M. J., Briggs, N. T., Kallin, E., D’Asaro, E. A., and Lee, C. M.: Particulate Organic Carbon and Inherent Optical Properties during 2008 North Atlantic Bloom Experiment: POC AND OPTICS-NAB08, J. Geophys. Res.-Oceans, 117, TS10, https://doi.org/10.1029/2011JC007771, 2012.
Chami, M. and Platel, M. D.: Sensitivity of the retrieval of the inherent optical properties of marine particles in coastal waters to the directional variations and the polarization of the reflectance, J. Geophys. Res.-Oceans, 112, TS11, 2007.
Claustre, H., Fell, F., Oubelkheir, K., Prieur, L., Sciandra, A., Gentili, B., and Babin, M.: Continuous monitoring of surface optical properties across a geostrophic front: Biogeochemical inferences. Limnol. Oceanogr., 45(2), 309–321, 2000.
Cole, J. J., Prairie, Y. T., Caraco, N. F., McDowell, W. H., Tranvik, L. J., Striegl, R. G., Duarte, C. M., Kortelainen, P.,

- Downing, J. A., Middelburg, J. J., and Melack, J.: Plumbing the Global Carbon Cycle: Integrating Inland Waters into the Terrestrial Carbon Budget, *Ecosystems*, 10, 172–185, <https://doi.org/10.1007/s10021-006-9013-8>, 2007.
- D'Alimonte, D., Zibordi, G., Kajiyama, T., and Berthon, J. F.: Comparison between MERIS and regional high-level products in European seas, *Remote Sens. Environ.*, 140, 378–395, 2014.
- Defoin-Platel, M. and Chami, M.: How ambiguous is the inverse problem of ocean color in coastal waters?, *J. Geophys. Res.-Oceans*, 112, TS12, 2007.
- Doerffer, R. and Schiller, H.: The MERIS Case 2 water algorithm, *Int. J. Remote Sens.*, 28, 517–535, 2007.
- Doron, M., Babin, M., Mangin, A., and Hembise, O.: Estimation of light penetration, and horizontal and vertical visibility in oceanic and coastal waters from surface reflectance, *J. Geophys. Res.-Oceans*, 112, TS13, 2007.
- Doron, M., Babin, M., Hembise, O., Mangin, A., and Garnesson, P.: Ocean transparency from space: Validation of algorithms estimating Secchi depth using MERIS, MODIS and SeaWiFS data, *Remote Sens. Environ.*, 115, 2986–3001, 2011.
- Dransfeld, S., Tatnall, A. R., Robinson, I. S., and Mobley, C. D.: Prioritizing ocean colour channels by neural network input reflectance perturbation, *Int. J. Remote Sens.*, 26, 1043–1048, 2005.
- Fell, F.: Oceanic Irradiance Profile Processing, Zenodo [code], <https://doi.org/10.5281/zenodo.8096682>, 2023. TS14
- Ferrari, G. M.: The Relationship between Chromophoric Dissolved Organic Matter and Dissolved Organic Carbon in the European Atlantic Coastal Area and in the West Mediterranean Sea (Gulf of Lions), *Mar. Chem.*, 70, 339–357, [https://doi.org/10.1016/S0304-4203\(00\)00036-0](https://doi.org/10.1016/S0304-4203(00)00036-0), 2000.
- Ferrari, G. M., Bo, F. G., and Babin, M.: Geo-Chemical and Optical Characterizations of Suspended Matter in European Coastal Waters, *Estuar. Coast. Shelf S.*, 57, 17–24, [https://doi.org/10.1016/S0272-7714\(02\)00314-1](https://doi.org/10.1016/S0272-7714(02)00314-1), 2003.
- GEBCO Bathymetric Compilation Group 2021 TS15: The GEBCO_2021 Grid – a Continuous Terrain Model of the Global Oceans and Land, TS16, <https://doi.org/10.5285/C6612CBE-50B3-0CFF-E053-6C86ABC09F8F>, 2021. TS17.
- Gordon, H. R. and Morel, A. Y.: Remote Assessment of Ocean Color for Interpretation of Satellite Visible Imagery: A Review, Springer US, New York, NY, TS18, 1983.
- Groom, S., Martinez-Vicente, V., Fishwick, J., Tilstone, G., Moore, G., Smyth, T., and Harbour, D.: The western English Channel observatory: Optical characteristics of station L4, *J. Marine Syst.*, 77, 278–295, 2009.
- Guthrie, W. F.: NIST/SEMATECH e-Handbook of Statistical Methods (NIST Handbook 151), TS19, <https://doi.org/10.18434/M32189>, 2012.
- Hedges, J., Keil, R., and Benner, R.: What Happens to Terrestrial Organic Matter in the Ocean?, *Org. Geochem.*, 27, 195–212, [https://doi.org/10.1016/S0146-6380\(97\)00066-1](https://doi.org/10.1016/S0146-6380(97)00066-1), 1997.
- Jamet, C., Loisel, H., and Dessailly, D.: Retrieval of the spectral diffuse attenuation coefficient K_d (λ) in open and coastal ocean waters using a neural network inversion, *J. Geophys. Res.-Oceans*, 117, TS20, 2012.
- Jerlov, N.: Optical Oceanography, Elsevier Publishing Company, New York, TS21, 1968.
- Kratzer, S. and Moore, G.: Inherent optical properties of the baltic sea in comparison to other seas and oceans, *Remote Sens.*, 10, 418, TS22, 2018.
- Lee, Z., Carder, K. L., Mobley, C. D., Steward, R. G., and Patch, J. S.: Hyperspectral Remote Sensing for Shallow Waters. I. A Semianalytical Model, *Appl. Optics*, 37, 6329, <https://doi.org/10.1364/AO.37.006329>, 1998.
- Loisel, H., Stramski, D., Mitchell, B. G., Fell, F., Fournier-Sicre, V., Lemasse, B., and Babin, M.: Comparison of the ocean inherent optical properties obtained from measurements and inverse modeling, *Appl. Optics*, 40, 2384–2397, 2001.
- Loisel, H., Vantrepotte, V., Ouillon, S., Ngoc, D. D., Herrmann, M., Tran, V., TS23..., and Van Nguyen, T.: Assessment and analysis of the chlorophyll- a concentration variability over the Vietnamese coastal waters from the MERIS ocean color sensor (2002–2012), *Remote Sens. Environ.*, 190, 217–232, 2017.
- Loisel, H., Stramski, D., Dessailly, D., Jamet, C., Li, L., and Reynolds, R. A.: An inverse model for estimating the optical absorption and backscattering coefficients of seawater from remote-sensing reflectance over a broad range of oceanic and coastal marine environments, *J. Geophys. Res.-Oceans*, 123, 2141–2171, 2018.
- Massicotte, P.: PMassicotte/Coastlooc_data_paper: V1.0.0, Zenodo [code], <https://doi.org/10.5281/zenodo.7708653>, 2023a.
- Massicotte, P.: PMassicotte/coastlooc_data_paper: ESSD revision round 1 (v1.1.0), Zenodo [code], <https://doi.org/10.5281/zenodo.8091717>, 2023b. TS24
- Massicotte, P., Stedmon, C., and Markager, S.: Spectral Signature of Suspended Fine Particulate Material on Light Absorption Properties of CDOM, *Mar. Chem.*, 196, TS25, <https://doi.org/10.1016/j.marchem.2017.07.005>, 2017.
- Massicotte, P., Babin, M., Fell, F., Fournier-Sicre, V., and Doxaran, D.: The COASTLOOC Project Dataset, SEANOE [data set], <https://doi.org/10.17882/93570>, 2023.
- Matsuoka, A., Hill, V., Huot, Y., Babin, M., and Bricaud, A.: Seasonal variability in the light absorption properties of western Arctic waters: Parameterization of the individual components of absorption for ocean color applications, *J. Geophys. Res.-Oceans*, 116, TS26, 2011.
- Matsuoka, A., Babin, M., Doxaran, D., Hooker, S. B., Mitchell, B. G., Bélanger, S., and Bricaud, A.: A synthesis of light absorption properties of the Arctic Ocean: application to semianalytical estimates of dissolved organic carbon concentrations from space, *Biogeosciences*, 11, 3131–3147, <https://doi.org/10.5194/bg-11-3131-2014>, 2014.
- Morel, A. and Bélanger, S.: Improved Detection of Turbid Waters from Ocean Color Sensors Information, *Remote Sens. Environ.*, 102, 237–249, <https://doi.org/10.1016/j.rse.2006.01.022>, 2006.
- Morel, A. and Prieur, L.: Analysis of Variations in Ocean Color: Ocean Color Analysis, *Limnol. Oceanogr.*, 22, 709–722, <https://doi.org/10.4319/lo.1977.22.4.0709>, 1977.
- Neukermans, G., Loisel, H., Mériaux, X., Astoreca, R., and Mc Kee, D.: In situ variability of mass-specific beam attenuation and backscattering of marine particles with respect to particle size, density, and composition, *Limnol. Oceanogr.*, 57, 124–144, 2012.
- O'Reilly, J. E. and Werdell, P. J.: Chlorophyll Algorithms for Ocean Color Sensors - OC4, OC5 & OC6, *Remote Sens. Environ.*, 229, 32–47, <https://doi.org/10.1016/j.rse.2019.04.021>, 2019.

- Oubelkheir, K., Claustre, H., Bricaud, A., and Babin, M.: Partitioning total spectral absorption in phytoplankton and colored detrital material contributions, *Limnol. Oceanogr.-Methods*, 5, 384–395, 2007.
- 5 R Core Team: R: A Language and Environment for Statistical Computing, R Foundation for Statistical Computing, Vienna, Austria, 2023.
- Sathyendranath, S.: Remote Sensing of Ocean Colour in Coastal, and Other Optically-Complex, Waters, Reports of the International Ocean-Colour Coordinating Group, No. 3, IOCCG, **TS27**, Dartmouth, Canada, 2000.
- 10 Schroeder, T., Behnert, I., Schaale, M., Fischer, J., and Doerffer, R.: Atmospheric correction algorithm for MERIS above case-2 waters, *Int. J. Remote Sens.*, 28, 1469–1486, 2007.
- 15 Schroeder, T., Schaale, M., Lovell, J., and Blondeau-Patissier, D.: An ensemble neural network atmospheric correction for Sentinel-3 OLCI over coastal waters providing inherent model uncertainty estimation and sensor noise propagation, *Remote Sens. Environ.*, 270, 112848, **TS28**, 2022.
- 20 Shahraiyni, T. H., Schaale, M., Fell, F., Fischer, J., Preusker, R., Vatandoust, M., **TS29**... and Tavakoli, A.: Application of the Active Learning Method for the estimation of geophysical variables in the Caspian Sea from satellite ocean colour observations, *Int. J. Remote Sens.*, 28, 4677–4683, 2007.
- 25 Stramski, D., Reynolds, R. A., Babin, M., Kaczmarek, S., Lewis, M. R., Röttgers, R., Sciandra, A., Stramska, M., Twardowski, M. S., Franz, B. A., and Claustre, H.: Relationships between the surface concentration of particulate organic carbon and optical properties in the eastern South Pacific and eastern Atlantic Oceans, *Biogeosciences*, 5, 171–201, <https://doi.org/10.5194/bg-5-171-2008>, 2008.
- 30 Sugihara, S., Kishino, M., and Okami, N.: Contribution of Raman Scattering to Upward Irradiance in the Sea, *Journal of the Oceanographical Society of Japan*, 40, 397–404, <https://doi.org/10.1007/BF02303065>, 1984.
- 35 Tassan, S. and Ferrari, G. M.: An Alternative Approach to Absorption Measurements of Aquatic Particles Retained on Filters, *Limnol. Oceanogr.*, 40, 1358–1368, <https://doi.org/10.4319/lo.1995.40.8.1358>, 1995.
- 40 Tassan, S. and Ferrari, G. M.: Measurement of Light Absorption by Aquatic Particles Retained on Filters: Determination of the Optical Pathlength Amplification by the ‘Transmittance-Reflectance’ Method, *J. Plankton Res.*, 20, 1699–1709, <https://doi.org/10.1093/plankt/20.9.1699>, 1998.
- 45 Tassan, S. and Ferrari, G. M.: A sensitivity analysis of the ‘Transmittance-Reflectance’ method for measuring light absorption by aquatic particles, *J. Plankton Res.*, 24, 757–774, 2002.
- 50 Tassan, S. and Ferrari, G. M.: Variability of Light Absorption by Aquatic Particles in the Near-Infrared Spectral Region, *Appl. Optics*, 42, 4802, <https://doi.org/10.1364/AO.42.004802>, 2003.
- Tassan, S., Ferrari, G. M., Bricaud, A., and Babin, M.: Variability of the amplification factor of light absorption by filter-retained aquatic particles in the coastal environment, *J. Plankton Res.*, 22, 55 659–668, 2000.
- Van Der Linde, D.: Protocol for Determination of Total Suspended Matter in Oceans and Coastal Zones, Tech. Rep. I.98, **TS30**, 1998.
- Vargas, M., Brown, C. W., and Sapiano, M. R. P.: Phenology of Marine Phytoplankton from Satellite Ocean Color Measurements, *Geophys. Res. Lett.*, 36, L01608, <https://doi.org/10.1029/2008GL036006>, 2009.
- 60 Vidussi, F., Claustre, H., Bustillos-Guzmán, J., Cailliau, C., and Marty, J.-C.: Determination of Chlorophylls and Carotenoids of Marine Phytoplankton: Separation of Chlorophyll *a* from Divinylchlorophyll *a* and Zeaxanthin from Lutein, *J. Plankton Res.*, 18, 2377–2382, <https://doi.org/10.1093/plankt/18.12.2377>, 1996.
- Wei, J., Wang, M., Jiang, L., Yu, X., Mikelsons, K., and Shen, F.: Global estimation of suspended particulate matter from satellite ocean color imagery, *J. Geophys. Res.-Oceans*, 126, e2021JC017303, **TS31**, 2021.
- 70 Yu, X., Salama, M. S., Shen, F., and Verhoef, W.: Retrieval of the diffuse attenuation coefficient from GOCI images using the 2SeaColor model: A case study in the Yangtze Estuary, *Remote Sens. Environ.*, 175, 109–119, 2016.
- 75 Yu, X., Lee, Z., Shen, F., Wang, M., Wei, J., Jiang, L., and Shang, Z.: An empirical algorithm to seamlessly retrieve the concentration of suspended particulate matter from water color across ocean to turbid river mouths, *Remote Sens. Environ.*, 235, 111491, **TS32**, 2019.
- Zhang, T. and Fell, F.: An approach to improving the retrieval accuracy of oceanic constituents in Case II waters, *J. Ocean U. China*, 3, 220–224, 2004.
- Zhang, T. and Fell, F.: An empirical algorithm for determining the diffuse attenuation coefficient Kd in clear and turbid waters from spectral remote sensing reflectance, *Limnol. Oceanogr.-Methods*, 5, 457–462, 2007.
- Zhang, T., Fell, F., Liu, Z. S., Preusker, R., Fischer, J., and He, M. X.: Evaluating the performance of artificial neural network techniques for pigment retrieval from ocean color in Case I waters, *J. Geophys. Res.-Oceans*, 108, **TS33**, 2003.
- Zheng, G. and Stramski, D.: A model based on stacked-constraints approach for partitioning the light absorption coefficient of seawater into phytoplankton and non-phytoplankton components, *J. Geophys. Res.-Oceans*, 118, 2155–2174, 2013.

Remarks from the language copy-editor

- CE1** Please note the above changes to the town names in affiliations 3 and 4.
- CE2** Please note in this paper the terms that have been hyphenated when functioning as adjectives and left unhyphenated when functioning as nouns.
- CE3** Additional changes were made to Figs. 5 and 8 for consistency with the main text.
- CE4** Please confirm.
- CE5** Please check: should this be *a*?
- CE6** Do you mean "carbon" here (in line with the following abbreviation)?
- CE7** What does "M" stand for here?
- CE8** Please define this name here.
- CE9** Should this be "hypochlorite"?
- CE10** Please check the edits to this sentence as they might not show up in the track-changes .pdf file.
- CE11** Please check and confirm this word: it does not seem to correspond to anything similar in the paper.
- CE12** Do you mean "floor" here?
- CE13** Please confirm.
- CE14** Please define this abbreviation here.
- CE15** Please define this abbreviation here.

Remarks from the typesetter

- TS1** The composition of Figs. 2–9 has been adjusted to our standards.
- TS2** Please check change due to guidelines.
- TS3** Please provide a reference list entry including creators, title, and date of last access.
- TS4** Please note that all references mentioned in this table have been moved to the reference list and only the citations are listed here.
- TS5** Please ensure that any data sets and software codes used in this work are properly cited in the text and included in this reference list. Thereby, please keep our reference style in mind, including creators, titles, publisher/repository, persistent identifier, and publication year. Regarding the publisher/repository, please add "[data set]" or "[code]" to the entry (e.g., Zenodo [code]).
- TS6** Please provide the page range or article number with DOI.
- TS7** Please provide DOI.
- TS8** Please provide the page range or article number with DOI.
- TS9** Please provide DOI.
- TS10** Please provide article number or page range.
- TS11** Please provide the page range or article number with DOI.
- TS12** Please provide the page range or article number with DOI.
- TS13** Please provide the page range or article number with DOI.
- TS14** Please confirm.
- TS15** Please check and confirm authorship change.
- TS16** Please add the name of publisher/publishing institution and place of publication.
- TS17** Please ensure that any data sets and software codes used in this work are properly cited in the text and included in this reference list. Thereby, please keep our reference style in mind, including creators, titles, publisher/repository, persistent identifier, and publication year. Regarding the publisher/repository, please add "[data set]" or "[code]" to the entry (e.g. Zenodo [code]).
- TS18** Please provide persistent identifier (ISBN or DOI preferred.)
- TS19** Please add the name of publisher/publishing institution and place of publication.
- TS20** Please provide the page range or article number with DOI.
- TS21** Please provide persistent identifier (ISBN or DOI preferred.)
- TS22** Please provide DOI.
- TS23** Please provide the complete author list.
- TS24** Please confirm.
- TS25** Please provide article number or page range.
- TS26** Please provide the page range or article number with DOI.

- TS27 Please add the name of publisher/publishing institution.
- TS28 Please provide DOI.
- TS29 Please provide the complete author list.
- TS30 Please add the name of publisher/publishing institution and place of publication.
- TS31 Please provide DOI.
- TS32 Please provide DOI.
- TS33 Please provide the page range or article number.